Journal of Colloid and Interface Science 657 (2024) 352–362

Contents lists available at ScienceDirect

Journal of Colloid And Interface Science

journal homepage: www.elsevier.com/locate/jcis

Insights into the emulsification mechanism of the surfactant-like protein oleosin

Lorenz Plankensteiner [a,b], Marie Hennebelle [b], Jean-Paul Vincken [b], Constantinos V. Nikiforidis [a,*]

[a] Laboratory of Biobased Chemistry and Technology, Wageningen University, the Netherlands
[b] Laboratory of Food Chemistry, Wageningen University, the Netherlands

GRAPHICAL ABSTRACT

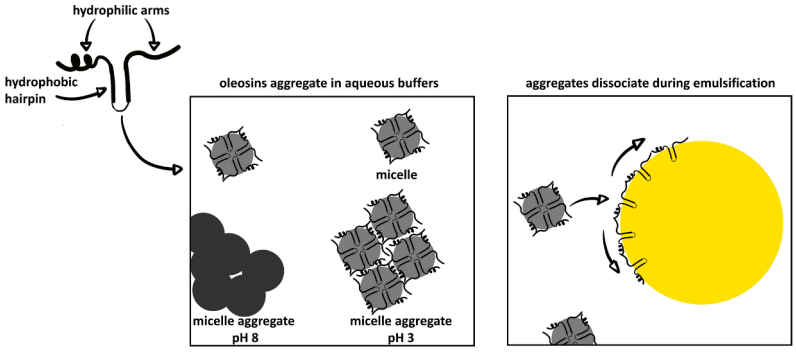

ARTICLE INFO

Keywords:
Oleosin
Lipid droplet
Emulsion
Emulsifier
Protein
Micelle
Oleosome
Surfactant

ABSTRACT

Oleosins are proteins with a unique central hydrophobic hairpin designed to stabilize lipid droplets (oleosomes) in plant seeds. For efficient droplet stabilization, the hydrophobic hairpin with a strong affinity for the apolar droplet core is flanked by hydrophilic arms on each side. This gives oleosins a unique surfactant-like shape making them a very interesting protein. In this study, we tested if isolated oleosins retain their ability to stabilize oil-in-water emulsions, and investigated the underlying stabilization mechanism. Due to their surfactant-like shape, oleosins when dispersed in aqueous buffers associated to micelle-like nanoparticles with a size of ~33 nm. These micelles, in turn, clustered into larger aggregates of up to 20 μm. Micelle aggregation was more extensive when oleosins lacked charge. During emulsification, oleosin micelles and micelle aggregates dissociated and mostly individual oleosins adsorbed on the oil droplet interface. Oleosins prevented the coalescence of the oil droplets and if sufficiently charged, droplet flocculation as well.

* Corresponding author.
E-mail address: costas.nikiforidis@wur.nl (C.V. Nikiforidis).

https://doi.org/10.1016/j.jcis.2023.11.165
Received 21 July 2023; Received in revised form 23 October 2023; Accepted 26 November 2023
Available online 30 November 2023

1. Introduction

Oleosins are unique proteins present in plant seeds, that have a surfactant-like structure consisting of hydrophilic arms that flank a central hydrophobic hairpin. This structure is crucial for its role in stabilizing the lipid storage droplets called oleosomes [26,45,46]. Oleosins are believed to protect oleosomes from coalescing during extreme environmental conditions, like desiccation to moisture levels as low as 5–10 wt%, freezing winters, or several years of storage in a dry state until rehydration during seed germination [32,40].

The hydrophobic hairpin of oleosins is ~ 72 residues long and contains a proline knot with 12 highly conserved amino acid residues (PX_5SPX_3P, with X being a non-polar amino acid) that forces a 180° turn, giving the hairpin-like structure [6,19]. The exact secondary structure of the hairpin is still not established, however, recent experimental and modeling data suggest two alpha helixes that are connected via the proline knot [6,19,22]. In the native environment, the hydrophobic hairpin is believed to anchor into the triacylglyceride core of oleosomes [19,20]. The hydrophilic arms are facing the bulk phase and probably protecting oleosomes from coalescence [45,46].

The role of oleosins in stabilizing lipid droplets in seeds suggests that they might also be of great use in applications like oil-in-water emulsions. While *in vivo* oleosins are cotranslationally inserted on the interface of oleosomes during their formation [6,16,19], once isolated they need to be delivered to the interface via one of the two emulsion phases. Disadvantageously, isolated oleosins have low solubility in water and most organic solvents due to their highly amphiphilic structure [15,35]. In water, oleosins assemble into nano- and microsized aggregates due to hydrophobically-driven interactions [27,37].

Currently, it is unknown how these aggregates are affecting the emulsification performance and emulsification mechanism of oleosins. While pure oleosins (isolated from oilseeds or recombinantly produced), either alone or in combination with phospholipids, have been used earlier to stabilize oil-in-water emulsions, limited insights into the underlying stabilization mechanism are available [12,23,33,35,36,45]. Particularly, it is unclear whether the emulsion interface is stabilized by oleosin aggregates or by individual oleosins.

Therefore, in this work, we aimed to unveil the mechanism by which isolated oleosins stabilize an oil-in-water emulsion. Rapeseed oleosins were dispersed in aqueous buffers at pH 3 and pH 8 to modulate the charge of oleosins and investigate how that affects their aggregation behavior. pH 3 is far from and pH 8 close to the isoelectric point range (7–10) that was previously calculated from the amino acid sequences of rapeseed oleosins [21]. Then, oil-in-water emulsions were made with different oleosin concentrations to determine which oleosin concentration was sufficient for the stabilization of the created interface. The microstructure of the droplets was imaged with Confocal Laser Scanning Microscopy (CLSM). Finally, experiments were combined with theoretical calculations to understand if oleosins stabilized the emulsions as aggregates or as individual proteins.

2. Experimental

2.1. Materials

Refined rapeseed oil was bought from a local supermarket. Rapeseeds (*B. napus*, variety Alizze) were obtained from a European seed producer and stored at −20 °C until use. Organic solvents were purchased from Biosolve (Valkenswaard, The Netherlands). Other chemicals were sourced from Merck (Darmstadt, Germany). All aqueous solutions and dispersions were made with Milli-Q water (Merck, Darmstadt, Germany).

2.2. Oleosome and oleosin extraction

Oleosins were extracted from rapeseed according to our recently published protocol [37]. First, rapeseeds were soaked in 0.1 M $NaHCO_3$ (pH 9.5) at a seed-to-solution ratio of 1:7 (w/w) for 16 h at 4 °C. The mixture was ground in a blender (Waring Commercial 7011HS, Torrington, Connecticut, USA) for 2 min at maximum speed and then filtered through cheesecloth using a vacuum pump. The resulting filtrate was centrifuged at 10,000x*g* for 30 min at 4 °C to separate oleosomes from other seed materials. After centrifugation, the oleosome-rich top layer was collected. The oleosomes were further washed with 0.1 M $NaHCO_3$ solution (pH 9.5) and then with water, both at a 1:4 (w/w) cream-to-solution ratio. Each washing step was followed by the same centrifugation and collection step as described earlier. The top layer collected after the final washing represented the oleosome cream. It was used as is for experiments on native oleosomes or frozen at −30 °C for the oleosin extraction.

After thawing, the oleosome cream was mixed with methanol in a 1:2 w/v ratio and incubated for 10 min at room temperature. The mix was then centrifuged for 10 min at 4,700x*g* and the top methanol phase was removed. The pellet was washed three additional times with the same volume of methanol. After the methanol washings, the pellet was washed four times with hexane and finally, three times with ethanol, following the same procedure. The collected pellet was then dispersed in water with a sonication bath running at 40 kHz (M2800, Branson, Ferguson, USA) for 5 min. The mixture was frozen and lyophilized, resulting in oleosins. The homogeneity of the obtained oleosins was confirmed with SDS-PAGE (Fig. S1 in supplemental information) and the purity with the Dumas method using a nitrogen-protein conversion factor of 5.7 as described previously [37]. Oleosins were homogenous with a main band at 17 kDa and had a protein purity of 88.4 wt%. Additionally, we checked with ^{31}P NMR for traces of phospholipids in the isolated oleosins as described in our other recently submitted manuscript [18]. Traces of 1–2 wt% of phosphatidylinositol (PI) were present. Isolated oleosinswere stored at −30 °C until further use.

2.3. Preparation of oleosin dispersions

Oleosin dispersions (DS) were prepared by dispersing oleosins at different protein concentrations (0.002–17 g/L) in 10 mM phosphate buffer (ionic strength adjusted to 30 mM with NaCl) at pH 3 or 8. The pH of the dispersions was measured, and if necessary, adjusted with 1 M HCl or NaOH solution to reach pH 3 or 8. The oleosin dispersions were shaken or stirred for 12 h at 4 °C and then sonicated at 40 kHz for 10 min in a sonication bath (M2800, Branson, Ferguson, USA).

2.4. Oleosin emulsions

The oil-in-water emulsions (E) were prepared in a two-step process. First, rapeseed oil was mixed with oleosin dispersions and pre-emulsified with an Ultra-Turrax (IKA T 25 Ultra Turrax, Staufen, Germany) for 1 min at 9,500 rpm. Then, the mix was passed through a lab homogenizer (Delta Instruments LaboScope Homogenizer, Northvale, New Jersey, USA) at 150 bar for 10 passes. The heating of the sample was prevented by keeping it in an ice bath during homogenization. We decided to deliver oleosins to the droplet interface through the aqueous phase. This allowed the separation of unadsorbed oleosins from the emulsion droplets to determine the interfacial load as described later.

2.5. Native oleosome emulsions

Oleosomes were dispersed in 10 mM phosphate buffer (ionic strength adjusted to 30 mM with NaCl) at pH 8 to create a 10 wt% oil-in-water emulsion. The dispersion was mixed with an Ultra-Turrax for 1 min at the lowest speed (2,000 rpm) to get a homogenous preparation.

2.6. Transmission electron Microscopy (TEM)

Aliquots of 6 μL oleosins dispersions (0.85 g/L) were transferred onto

a carbon-coated hexagonal 400 mesh copper grid and left to adsorb for several minutes. Then, a filter paper was used to remove excess liquid and the grid was air dried for several minutes. Finally, the samples were imaged with a JEOL JEM1400 + microscope (JEOL Ltd., Tokyo, Japan) operating at 120 kV. Sizes of the nanosized oleosin particles (later called micelles) were estimated by measuring the maximum Feret diameters of 21 particles with the software FIJI (Scheindlin et al., 2012).

2.7. Dynamic light scattering (DLS)

Oleosin dispersions (0.85 g/L) were filtered through a 0.45 μm filter (Minisart® Cellulose-Acetate, Sartorius, Göttingen, Germany) to remove larger aggregates that otherwise would precipitate through gravitation. The size of the oleosins in the filtrate was determined with dynamic light scattering with a Zetasizer Nano ZS (Malvern Instruments, Worcestershire, UK). The refractive index of the dispersant was 1.33 (water), and the refractive index of oleosins was set to 1.45 according to the manufacturer's guidelines for proteins. Measurements were performed at 22 °C and the results were collected as averages of three sequential measurement runs.

2.8. Pyrene assay

The dependence of the fluorescence vibrational fine structure of pyrene on its surrounding polarity was used to determine the critical concentration for the formation of micelle-like particles of oleosins (CMC) [1,48]. A pyrene stock of 12 mM pyrene in ethanol was prepared of which 7 μL were mixed with 20 mL of the 10 mM phosphate buffer (pH 3 or pH 8). Then, this pyrene phosphate mix was combined in a 1:6 v/v ratio with oleosin dispersions. After an incubation of 1 h in the dark, the samples were transferred to quartz cuvettes and measured with a Fluorlog 322 spectrofluorometer (Horiba, Kyoto, Japan). Samples were excited at 334 nm and emission was measured at 360–400 nm (excitation slit, 5 nm; emission slit, 5 nm). The intensity of the first (I_1) and third (I_3) vibronic peak of pyrene emission were determined at 371 nm and 382 nm, respectively. The ratio of I_1/I_3 was plotted against the oleosin concentration and then fitted with a Boltzmann-type sigmoid function (equation (1) to determine the CMC [1,48].

$$\frac{I_1}{I_3} = \frac{A - B}{1 + e^{\frac{C_{oleosin} - x_0}{\Delta x}}} + B \tag{1}$$

Where A and B are the upper and lower limits of the sigmoid function, x_0 the inflection point of the function and Δx the range of oleosin concentration where the change of I_1/I_3 occurs. Depending on the ratio of $x_0/\Delta x$ this method can yield two CMC's, one at x_0 and one at $x_0 + 2\Delta x$. For the oleosins the ratios were < 10 and thus the CMC was determined at the inflection point x_0 [1].

2.9. Zeta-potential

For oleosin dispersions (0.85 g/L) the same filtration as for the DLS measurements was performed. Oleosin emulsions were diluted 1000 times in the corresponding buffers to prevent multiple scattering. The zeta-potential was determined with a Zetasizer Nano ZS (Malvern Instruments, Worcestershire, UK). Measurements were performed at 22 °C and the results were collected as averages of three sequential measurement runs.

2.10. Static Light Scattering (SLS) for droplet size distributions and calculation of the interfacial area

The droplet size distributions of oleosin emulsions were determined by laser diffraction using a Bettersizer S3 Plus (3P Instruments GmbH & Co. KG, Odelzhausen, Germany). A refractive index of 1.465 was used for the dispersed phase and the refractive index of water (1.33) was used for the continuous phase. The stirring speed was set to 1,600 rpm. Additional measurements were performed after mixing the emulsions with 1 wt% sodium dodecyl sulphate (SDS) in a ratio of 1:1 (v/v). SDS is known to break up droplet flocculates, allowing the measurement of the size of individual droplets. The results were reported as Sauter diameter ($d_{3,2}$) or volume-averaged diameter ($d_{4,3}$). The interfacial area of the emulsions was calculated based on the volume frequency distribution of the individual droplets (after mixing with SDS) according to equation (2). The droplet sizes were separated into 100 size bins.

$$interfacial\ area\ emulsion = \sum_{1}^{n} \frac{6 \times V \times freq_i}{d_{4,3\,i}} \tag{2}$$

Where V is the volume (m^3) of the dispersed phase (oil), $freq_i$ is the volume frequency for each droplet size bin and $d_{4,3i}$ is the volume averaged droplet diameter of each bin (m).

2.11. Critical oleosin concentration for emulsification

The critical (minimal) protein concentration (C_{cr}) needed to form emulsions with the minimum droplet size ($d_{3,2}$) was determined by making 1 wt% oil-in-water emulsions ($\varphi_{oil} = 0.01$) with different oleosin concentrations (0.085–1.7 g/L). The data were then multiplied by 10 to calculate the concentrations for 10 wt% emulsions ($\varphi_{oil} = 0.1$) and allow comparisons with other proteins, for which C_{cr} was previously reported for 10 wt% emulsions. Previous tests on whey protein emulsions demonstrated that such an extrapolation is possible [44]. The measured droplet size as a function of oleosin concentration ($C_{oleosin}$) was fitted with equation (3).

$$d_{3,2} = a^* \frac{1}{C_{oleosin}} + d_{3,2min} \tag{3}$$

where $d_{3,2}$ (μm) is the Sauter mean droplet diameter, $C_{oleosin}$ (g/L) is the oleosin concentration in the emulsion, and $d_{3,2min}$ (μm) is the minimum achievable droplet diameter with the used homogenizer settings. C_{cr} was defined as the concentration at which the derivative of the fitted function reached a value below −0.01, i.e., from this point on, the droplet diameter decreased<0.01 μm when increasing the oleosin concentration by 1 g/L. For investigating the stabilizing mechanism and the stability of the oleosin emulsions, 10 wt% oil-in-water emulsions ($\varphi_{oil} = 0.1$) were made with an oleosin concentration above C_{cr} of 12.75 g/L. All emulsions were prepared in duplicate. To test the physical stability of the emulsions they were stored for 7 days at 4 °C.

2.12. Confocal Laser Scanning Microscopy (CLSM)

Oleosin emulsions (1 mL) were stained with 7 μL of the lipophilic dye Nile Red (1 mg/mL in dimethyl sulfoxide), which co-localizes with triacylglycerides. Additionally, 7 μL of Fast Green FCF was added to indicate the location of proteins, as it electrostatically interacts with basic amino acids. The microstructure was imaged with a Confocal Laser Scanning Microscope (Leica SP8- SMD microscope, Leica Microsystems, Wetzlar, Germany) using a 63x magnification water immersion lens. Samples were excited at $\lambda = 488$ nm for Nile Red and $\lambda = 633$ nm for Fast Green, and the emission was recorded between 500 and 600 nm for Nile Red and between 650 and 700 for Fast Green. The images were processed with the software FIJI [39].

2.13. Interfacial load

Oleosin emulsions or native oleosome emulsions were centrifuged for 30 min at 21,000x*g* at 4 °C. This resulted in a three-phase system: a top layer of creamed intact oil droplets including adsorbed protein, a serum phase containing excess soluble protein and a pellet with excess insoluble proteins. To ensure that all the non-adsorbed protein was removed, the top cream layer was collected and further washed with

buffer by mixing it in a 1:10 w/w ratio with the corresponding phosphate buffer (pH 3 or 8). This was followed by another centrifugation for 30 min at 21,000xg at 4 °C. The washing of the cream layer was repeated until no more protein pellet was visible. Then, the dry matter- and protein content of the cream layer were determined and used to calculate the interfacial load with equation (4).

$$\Gamma = \frac{mass\ of\ adsorbed\ protein}{interfacial\ area\ of\ emulsion} \quad (4)$$

2.14. Theoretical calculation of oleosins size at the droplet interface

To get insights into the stabilizing mechanism, the size of oleosins at the interface was theoretically calculated using equation (5), which was adapted from previous research [38,42]. Oleosins were assumed to be disks on a two-dimensional interface.

$$oleosin\ diameter\ at\ interface = \frac{3}{2} * \frac{\Gamma_{exp}}{p^* \varphi_{max}} \quad (5)$$

Where Γ_{exp} is the experimentally determined interfacial load (mg/m^2), ρ is the oleosin density, assumed to be 1.45 g/cm^3 [14]and φ_{max} is the maximum packing density of oleosins at the interface. For $\varphi_{max,}$ two scenarios were considered: 1) the perfect packing of disks in a two-dimensional space ($\varphi_{max} = 0.91$) and 2) the random adsorption model ($\varphi_{max} = 0.547$) [43].

2.15. Interfacial adsorption

An automated drop tensiometer (ADT) (Teclis, Lyon, France) was used to examine the adsorption of oleosins at the oil–water interface. The oil phase consisted of rapeseed oil that was stripped from interfacial active impurities by mixing it with Florisil (100–200 mesh, magnesium silicate, Merck, Darmstadt, Germany) in a ratio of 2:1 (v/v). The mix was

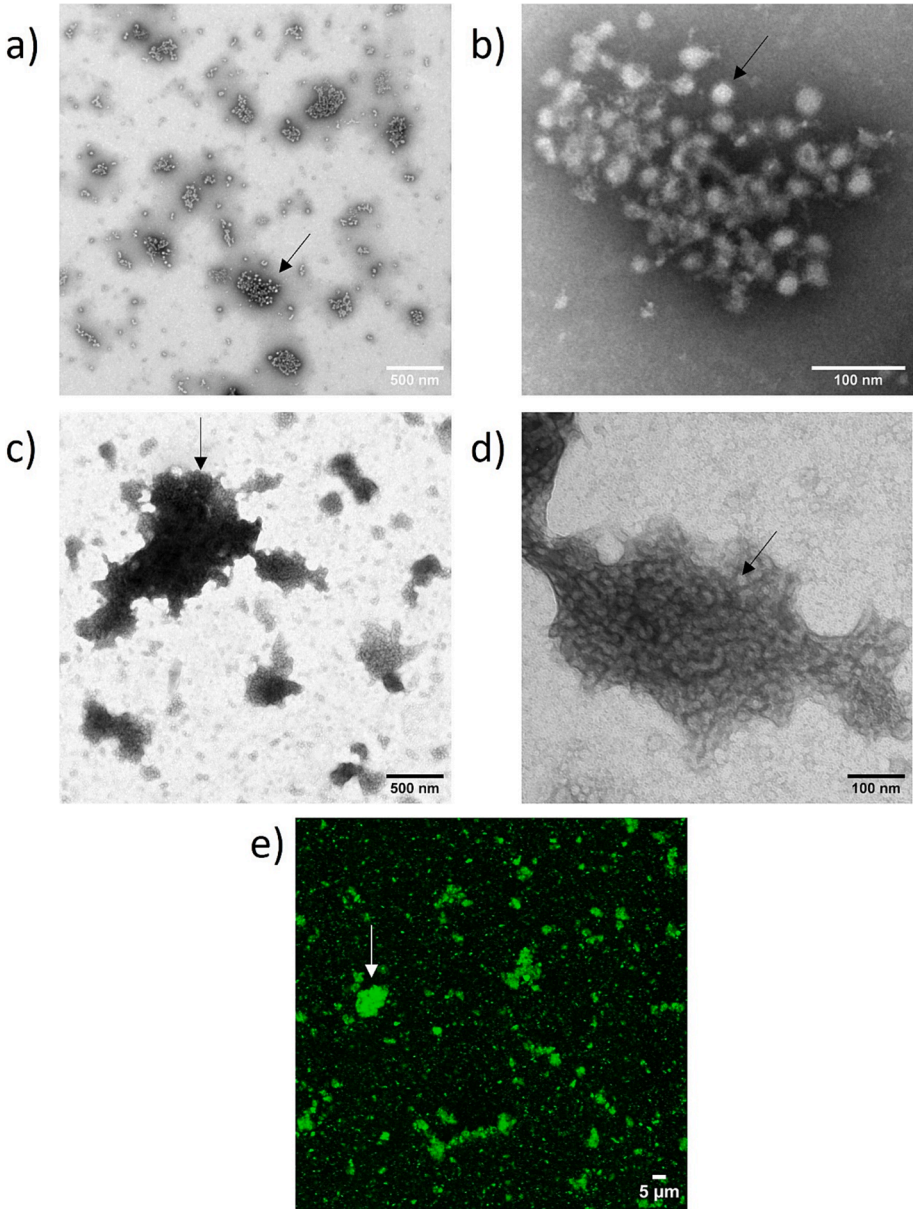

Fig. 1. Transmission Electron Microscopy (TEM) images of oleosin dispersions (1 mg/L) at pH 3 (a-b) and pH 8 (c-d). e) Confocal Laser Scanning Microscopy (CLSM) image of an oleosin dispersion at pH 3. The oleosin particles were localized with the fluorescent dye Fast Green. The arrows point to a microsized aggregate (a, c, e) or a nanosized oleosin aggregate (b, d).

covered in aluminum foil and shaken overnight at room temperature. Then the Florisil was removed by centrifuging the mix three times at 2,000x*g* for 20 min. The stripped oil was stored at −20 °C until use.

Oleosin dispersions (0.85 g/L) were filtered as described in the DLS section and then diluted to a protein concentration of 0.02 g/L, the final protein concentration was confirmed with the BCA assay as described by Plankensteiner et al. [37]. Then, a pendant drop (interfacial area of 30 mm^2) of the oleosin dispersion was formed in the stripped rapeseed oil with a coated G18 needle. To monitor the interfacial adsorption, the droplet shape changes were recorded by a camera, and then fitted to the Young-Laplace equation to determine the interfacial tension. Results are reported as interfacial pressure, which is defined as the difference of interfacial tension of the interface in the absence and presence of oleosin.

3. Results and discussion

3.1. Aggregation of oleosins in aqueous solutions

Oleosins were dispersed in aqueous solutions at pH 3 and 8 and their aggregation was visualized with TEM and CLSM. At both pH 3 and 8, oleosins formed aggregates with a broad size range from nano- to microscale. The smallest aggregates had maximum Feret diameters of ~ 0.03 μm (Fig. 1a, 1c), while the largest aggregates were almost 20 μm (Fig. 1e). The number of aggregates above the size of 1 μm was larger in the dispersion at pH 8 (DS_{pH8}) (Fig. 1a) compared to the one in the pH 3 dispersion (DS_{pH3}) (Fig. 1c). In addition, the aggregates at pH 8 had higher contrast, indicating higher electron density.

The inner structure of the aggregates of DS_{pH3} became clearer at high magnifications. The aggregates at above 100 nm were constructed of smaller nanosized particles with spherical to elliptical morphology (Fig. 1b). The size of the nanoparticles was estimated to be ~ 20–30 nm. Similarly, the inner structure of the aggregates of DS_{pH8} showed contrast differences, indicating that these aggregates were as well built from smaller nanosized particles (Fig. 1d). The structures were packed tighter, and the contrast between nanosized particles was not as high as in DS_{pH3} making the images more blurry and more difficult to observe the exact morphology of the nanoparticles. Nanoparticles were mainly visible in aggregates with Feret diameters below 1 μm and on the edges of aggregates above 1 μm (Fig. 1c). Some of the nanoparticles appeared spherical as in DS_{pH3}, while others appeared more elongated.

More quantitative characterization of the nanoparticles was achieved with Dynamic Light Scattering (DLS). To focus on the nanoparticles, the microsized aggregates (>450 nm) were removed before the measurements via filtration. The results were reported as number distribution (Fig. 2), to allow direct comparison with TEM and reduce the sensitivity to large aggregates, which would dominate volume and intensity distributions. Oleosin nanoparticles showed bimodal size distributions at both pH values. At pH 3, a broad main peak from 20 to 200 nm with a modal diameter at ~ 33 nm and a minor shoulder with ~ 14 nm was observed. The main peak at pH 8 ranged from 50 to 400 nm with the modal diameter at ~ 106 nm, while the minor peak had a maximum of ~ 33 nm. The common peak at ~ 33 nm (major peak in DS_{pH3} and minor in DS_{pH8}) most likely corresponded to the individual nanosized particles that were observed with TEM in DS_{pH3}. The presence of the ~ 33 nm large nanoparticles in DS_{pH8} supported the previous suggestion that the larger aggregates at pH 8 were made up from similar nanoparticles as found in DS_{pH3}. The sizes measured with DLS were slightly larger than with TEM, probably due to the hydration of the particles. The main peak of 106 nm of DS_{pH8} and the right tail of the main peak of DS_{pH3} represented aggregates of nanosized particles as indicated by the TEM images.

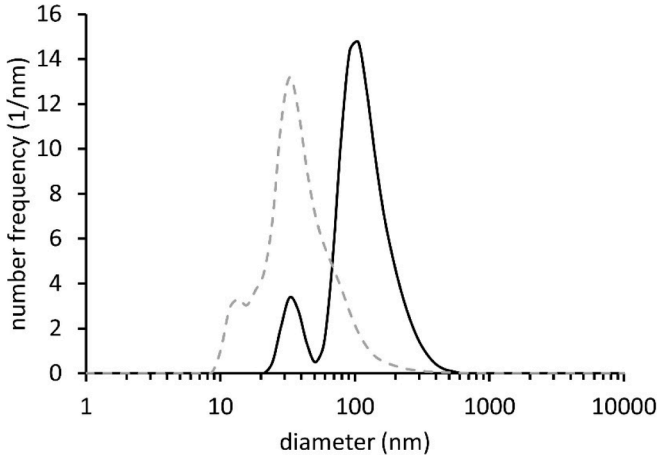

Fig. 2. Size distribution of oleosin nanoparticles and nanoparticle aggregates after filtration (sizes < 450 nm) at pH 3 (dashed grey line) and pH 8 (solid black line). Data are plotted as mean (n = 3).

Individual oleosin molecules aggregated in line with expectations from previous research [15,37,47]. Aggregation occurred on two length scales, an initial assembly to nanosized particles with a diameter of ~ 33 nm, which then further aggregated to form microsized assemblies of up to 20 μm. To confirm that these microsized aggregates were not an artifact of the drying during sample preparation, we imaged the same dispersions with CLSM (Fig. 1e).

We propose that the assembly of oleosins to nanosized particles was mainly driven by aggregation of their hydrophobic hairpins due to hydrophobically-driven interactions like it was described for truncated oleosin mutants and other surfactant proteins (e.g. hydrophobins) [8,13,47]. Exposure of the hydrophobic hairpin to water is energetically highly unfavorable, hence, oleosins aggregated into spherical and elongated micelle-like particles to prevent contact of the hairpins and water similar to surfactants [7,52]. In the following sections, the nanosized micelle-like particles of 33 nm will hence be called oleosin micelles, and their aggregates will be called micelle aggregates. The aggregation of oleosins on the two length scales at pH 8 and pH 3 is schematically presented in Fig. 3.

The critical concentration for the formation of oleosin micelles (CMC) was determined with the fluorescent probe pyrene, which changes its emission spectra (I_1/I_3 ratio) based on the local polarity [1]. The full plot of the I_1/I_3 ratio against oleosin concentration can be found in Fig. S2 in the supplemental information. The ratio I_1/I_3 decreased with increasing oleosin concentration, which indicated the formation of self-assembled structures with a hydrophobic core [25]. The CMC of oleosins was 0.02 g/L (~1.2 μM) at pH 3 and 0.04 mg/L (~2.4 μM) at pH 8, lower than the 5.7 μM reported previously for recombinant oleosins with a shortened hairpin [48]. The difference in CMC between oleosins with varying hairpin length indicates that the hydrophobic hairpin is the driver for aggregation, and longer hairpins lead to stronger attractive hydrophobically-driven interactions.

The aggregation number of oleosins in a micelle was estimated theoretically based on the size of an individual oleosin, as we were not able to separate sufficient individual oleosin micelles from the larger micelle aggregates for determining the aggregation number experimentally. The length of the hairpin could be roughly estimated to be ~ 6 nm and each arm to be ~ 10 nm from homology modeling and the structure of oleosin S3 predicted by Alpha Fold, S3 is one of the most abundant oleosins in *B.napus* (UniProt accession number C3S7G6) [19,24]. The exact configuration and packing of oleosins in the micelles were not known as the arms are likely flexible and may take different configurations. Therefore, the length of an oleosin (parallel to hairpin) could vary from ~ 6–16 nm, suggesting that two oleosins packed along the two-dimensional diameter of the micelles as schematically illustrated in Fig. 3.

The formation of micelle aggregates was pH dependent. To understand this pH dependence, the charge of the oleosin micelles was measured by determining the zeta-potential. The zeta-potential of DS_{pH3}

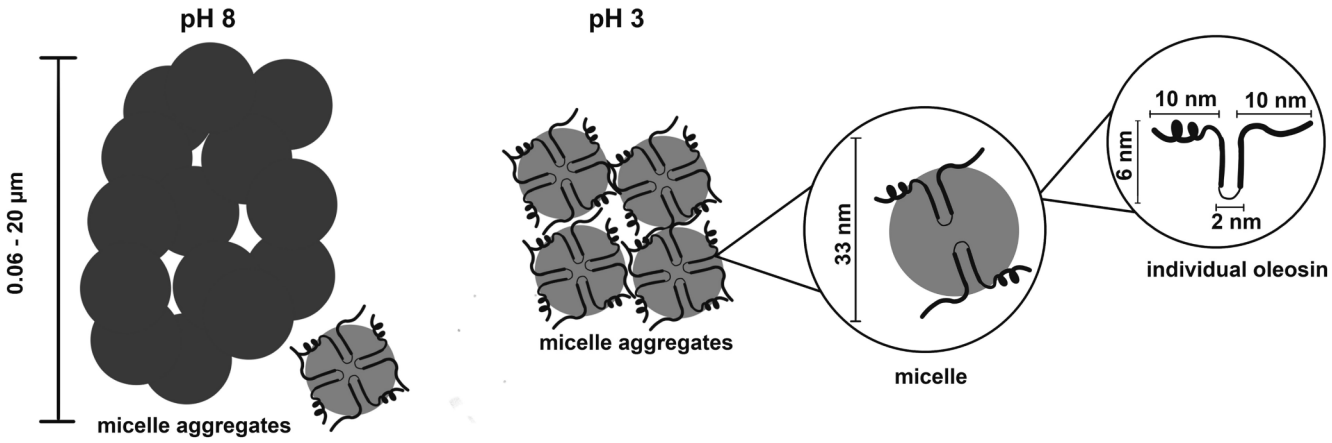

Fig. 3. Schematical representation of an individual oleosin and the formed micelle and micelle aggregates. The size of an individual oleosin was estimated from the homology modelling by Huang and Huang [19] and the structure of oleosin S3 (B.napus, Uniprot accession number C3S7G6) predicted by Alpha Fold [24]. The schematic representation is not to scale.

and DS_{pH8} were 20.1 ± 0.9 mV and −10.2 ± 0.3 mV, respectively. pH 8 was closer to the isoelectric point range (7–10) for rapeseed oleosins leading to less charge [21] and hence less electrostatic repulsion between oleosin micelles, increasing the tendency for micelle aggregation [31]. Larger and more densely packed aggregates formed. Although the exact attractive forces were not known, we speculated that hydrophobic patches on the surface of oleosin micelles could have driven their aggregation; these could come from some hydrophobic residues present on the oleosin arms, which would likely be on the surface of the particles [21,49].

3.2. Effect of oleosin concentration on oil droplet stabilisation

When making oil-in-water emulsions, sufficient emulsifier is needed to cover the created interface. If the emulsifier concentration is not sufficient, droplets coalesce during homogenization, until an interfacial area that can be sufficiently covered is reached [11,30]. To determine this critical concentration (C_{cr}) for rapeseed oleosins, emulsions were made with a series of oleosin concentrations (Fig. 4). Independent of the pH, the average individual droplet size decreased with increasing oleosin concentrations until a plateau was reached. From a first look at the measured $d_{3,2}$'s, the plateau appeared to be reached at ~ 2 g/L for E_{pH3} and at ~ 13 g/L for E_{pH8}. However, after closer inspection of the produced emulsions at pH 3, we could see that not all oil was incorporated at oleosin concentrations below 8 g/L. Therefore, we decided to fit the experimental data with equation (3) and calculate C_{cr} as the point where the individual droplet size decreased less than 0.01 µm after increasing the oleosin concentration by 1 g/L. C_{cr} was calculated to be at 8 g/L for E_{pH3} and 11 g/L for E_{pH8}, and at these concentrations, a $d_{3,2}$ of ~ 1.5 µm was achieved.

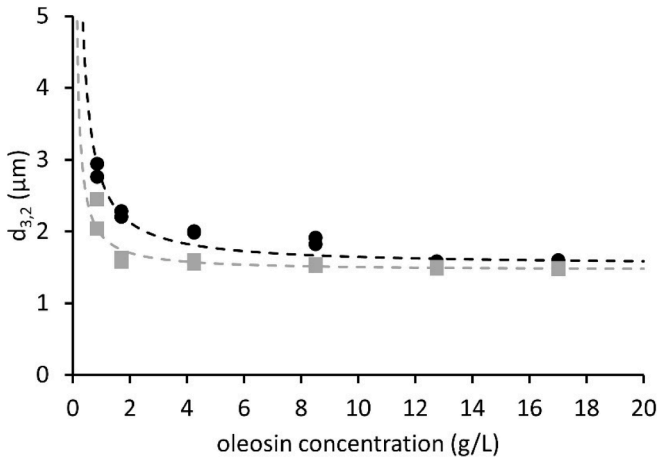

Fig. 4. Sizes of individual droplets ($d_{3,2}$) of a 10 wt% oil-in-water emulsions with different oleosin concentrations measured after mixing with 1 wt% SDS (1:1 v/v ratio). Grey squares represent emulsions at pH 3 and black circles at pH 8. The critical oleosin concentration (C_{cr}) was determined by fitting the experimental data with equation (2), the fits are plotted as dashed lines. C_{cr} was calculated to be 8 g/L for the emulsions at pH 3 and 11 g/L for the emulsions at pH 8.

The emulsions with C_{cr} had oil:protein weight ratios of 9.1 at pH 8 and 12.5 at pH 3. These oil:protein ratios were on the lower end of the ratios for other protein emulsifiers (e.g. ~ 100 for β-lactoglobulin, ~20 for ovalbumin, ~10 for lysozyme, ~25 for rubisco) that are necessary to create an oil-in-water emulsion ($\varphi_{oil} = 0.1$) with a $d_{3,2}$ of 1.5 µm [10,30]. All of these other proteins are more water soluble than oleosins making them more available to stabilize the created interface [34]. Oleosins instead, formed micelle aggregates in the aqueous phase which might have adsorbed as such or precipitated out, leading to the lower oil: protein ratios as in detail explained in the next paragraph. In E_{pH8}, the oleosin micelle aggregation was more extensive, which could partly explain the higher C_{cr} compared to E_{pH3}. Additionally, at pH 8, oleosins were less charged, leading to less intermolecular electrostatic repulsion and tighter packing at the interface and so, more oleosins were necessary to cover the interface [50].

We additionally compared the oil:protein of the oleosin emulsions to the one of native oleosomes. In native oleosomes, oleosins are suggested to form a monolayer that fully covers the interface [45]. Therefore, the comparison of the oil:protein ratios gave a first indication of the emulsification performance and mechanism of the isolated oleosins. The oil: protein ratio in native oleosomes was about four times higher (ratio of 38 for a $d_{3,2}$ of ~ 1.4 µm) than in the oleosin emulsions. Two possible reasons could lead to these differences: 1) only one fourth of the added oleosins adsorbed to the interface, while the rest was present as precipitates in the aqueous phase; 2) oleosins stabilized the interface as aggregates of which more are necessary to sufficiently cover the created interface.

3.3. Stabilizing mechanism of oleosins

More insights into the stabilizing mechanism of oleosins were obtained by imaging the microstructure of oleosin emulsions with CLSM. Oleosin emulsions ($\varphi_{oil} = 0.1$) were made with an oleosin concentration above C_{cr} to ensure full interfacial coverage. Nile Red and Fast Green were added as fluorescent probes to indicate the location of the oil (in

red) and proteins (in green). The droplets in E_{pH3} had a size of 1–2 μm and were well separated from each other (Fig. 5a-b). At pH 8, the droplet sizes were comparable to pH 3, but the droplets associated to large flocculates (Fig. 5c-d).

Next to the droplets, protein aggregates (in green in Fig. 5) were also visible in both E_{pH3} and E_{pH8}. These aggregates consisted of oleosin micelle aggregates (described in the previous section), as verified by comparing the images of the emulsions to the ones of oleosin dispersions (Fig. 1e). Little green was present at the interface of most droplets (Fig. 5). The interfacial oleosin layer might have been too thin, to allow abundant binding of fluorescent dye to the oleosins which led to weak visible emission. Most of the oleosins remained as aggregates in the continuous phase, rather than adsorbing to the droplet interface. This verified our assumption, that not all added oleosins were available to stabilize the droplets. Particularly, in E_{pH3}, the green signal came predominantly from the oleosin aggregates, and they were not associated with the droplets (Fig. 5a-b). In contrast, at pH 8, the oleosin aggregates were incorporated in the droplet flocculates and sometimes appeared to be at the interface (Fig. 5c-d). However, solely from the CLSM images, it was difficult to determine if the oleosin aggregates also play a role in stabilizing the droplets, or if they were just attached to the droplet interface.

To unveil if the interface was stabilized by individual oleosins or oleosin aggregates and to evidence that oleosins indeed adsorb to the interface, the interfacial loads (mass of oleosins per area of interface) were determined and used to theoretically calculate the size of oleosins

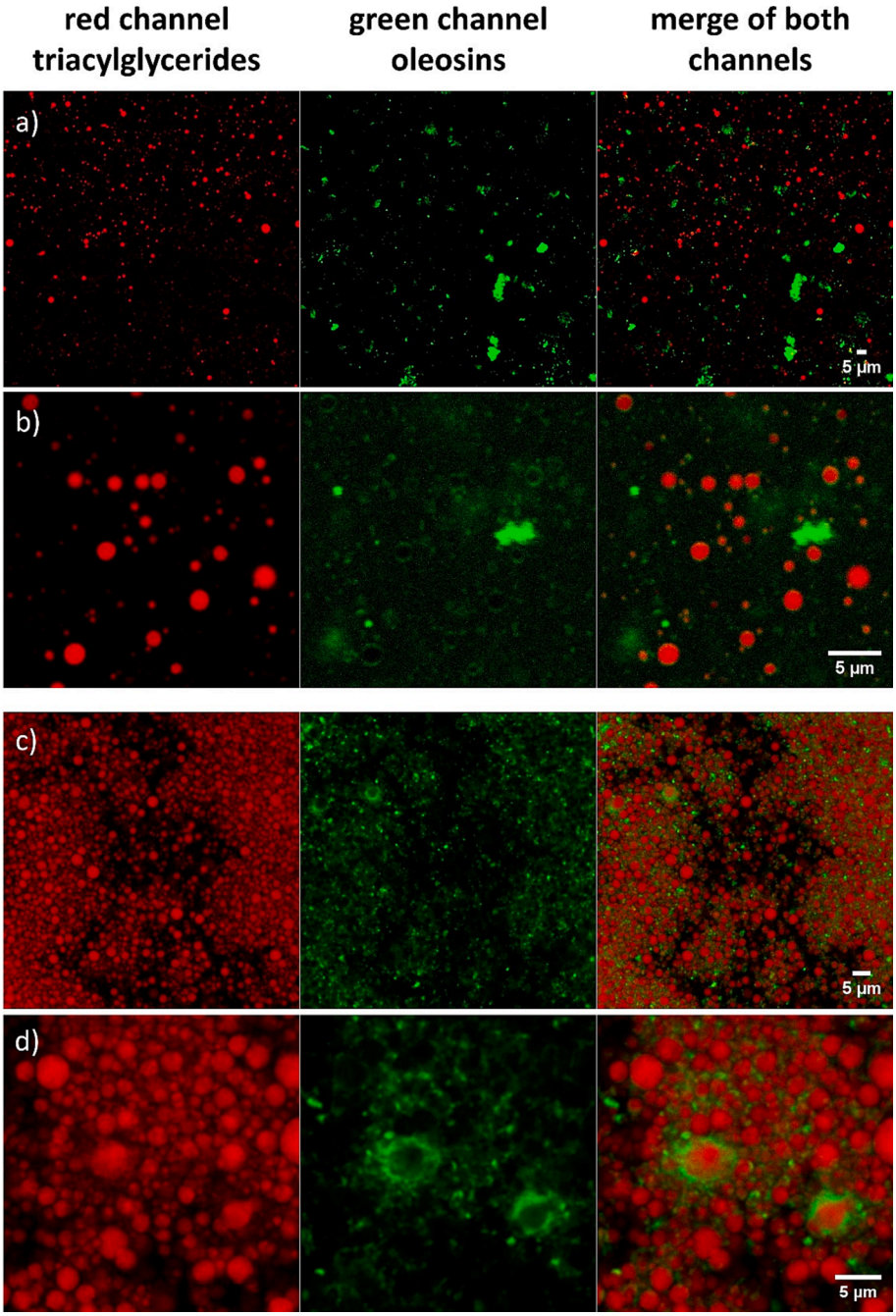

Fig. 5. Confocal Laser Scanning Microscopy (CLSM) images of oleosin emulsions. a-b shows the emulsion at pH 3, c-d the emulsion at pH 8. The fluorescent dyes Nile Red (in red) and Fast Green (in green) were used to indicate the location of triacylglycerides and proteins, respectively. For each emulsion, the red (left) and green (middle) channels are presented as well as a merged image of both channels (right).

at the droplet interface. The interfacial loads were 6.6 ± 0.2 mg/m^2 and 9.4 ± 0.5 mg/m^2 in E_{pH3} and E_{pH8}, respectively.

The interfacial loads were used to estimate the size of oleosins (equation (5). The packing density of proteins is dependent on their ability to diffuse on the interface and whether proteins can diffuse at the interface is still a matter of debate [3,9,43]. Therefore, two packing scenarios were considered. The first scenario assumed that oleosins were able to diffuse to the interface and thus reach the maximum packing density of discs on a two-dimensional area ($\varphi_{max} = 0.91$). For the second scenario, no diffusion was considered, and the randomly adsorbing oleosins would reach a jamming limit of interfacial packing ($\varphi_{max} = 0.547$) [43]. In scenario 1 ($\varphi_{max} = 0.91$), sizes for oleosins of 7.5 nm and 12.5 nm in E_{pH3} and E_{pH8} were calculated, while in scenario 2 ($\varphi_{max} = 0.547$), the sizes were estimated to be 10.7 and 17.8 nm, respectively. With both scenarios, the calculated sizes were close to the estimated diameter range of an oleosin monomer, which was estimated to be ~ 2 nm when only considering the hairpin, and up to 22 nm in the case of fully extended arms (Fig. 1f). This was the first indication that oleosin micelles and micelle aggregates might dissociate into monomers to stabilize the oil–water interface.

This hypothesis was further tested by comparing the interfacial load of the oleosin emulsions to the load of native oleosomes. If the aggregates dissociate when making emulsions, the oleosin emulsions were expected to have an almost identical interfacial load as native oleosomes. The interfacial protein load of native oleosomes was 6.0 ± 0.5 mg/m^2 which was almost identical to the interfacial load of E_{pH3} (6.6 ± 0.2 mg/m^2). Very likely, oleosin aggregates dissociated to monomers before adsorbing to the droplet interfaces of E_{pH3}, and then, packed to fully cover the interface like in native oleosomes. Considering the molecular weight of oleosins (~17 kDa), we calculated that each oleosin was covering 4.2 nm^2 of the interface in E_{pH3}, which was half of the proposed area for oleosins in maize oleosomes [45].

In E_{pH8}, ~50 % more oleosins were associated with the interface. This was partly derived from the lower charge and closer packing at the interface as described previously. In addition, next to individual oleosins, oleosin aggregates were present at the interface, which were likely incorporated in droplet flocculates or attached to the interfacial monolayer of oleosins as observed from the microstructure of E_{pH8} (Fig. 5c-d). The aggregates may have been strongly bound in the flocculates or to the interface of droplets; therefore, they were not removed during the washings and increased the measured interfacial load. Yet, the almost invisible protein layer for most droplets with CLSM (Fig. 5c-d) and the theoretically calculated size of oleosins at the interface, hinted that the interfacial layer consisted predominantly of oleosin monomers like in E_{pH3}. The aggregates were then additionally attached to this monolayer due to the lack of electrostatic repulsion in E_{pH8} as schematically illustrated in Fig. 7c.

To better understand the observed differences between pH 3 and pH 8, the interfacial adsorption of oleosin micelles and nanosized micelle aggregates to the oil–water interface was investigated. The obtained interfacial pressures are plotted as a function of the adsorption time in Fig. 6. At pH 8 oleosins adsorbed much faster to the interface than at pH 3 and reached a more than twice as high interfacial pressure after 2 h of adsorption.

As described previously, at pH 3 oleosin micelles aggregated less extensively than at pH 8 due to the higher absolute charge. Therefore, we initially expected faster adsorption at pH 3 based on the smaller sizes of oleosin aggregates at this pH. However, according to our measurements, aggregation size was not the factor determining fast adsorption, at both pH's probably sufficient oleosin micelles and small micelle aggregates were available to rapidly adsorb to the interface. Instead, charge appeared to determine the adsorption kinetics, since oleosins adsorbed much slower at pH 3. The increased charge at pH 3 likely increased the energetic barrier for adsorption leading to slower adsorption kinetics [5,50]. The lower plateau pressure that was reached at pH 3 after 2 h, was an additional indication that less oleosins adsorbed

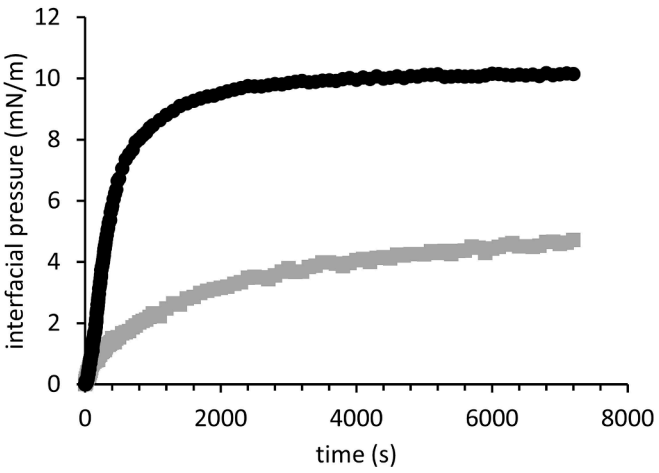

Fig. 6. Interfacial pressure as a function of time for oil–water interfaces stabilized by oleosin micelles and nanosized micelle aggregates measured with automated drop tensiometry (ADT). Grey squares represent the adsorption at pH 3 and black circles at pH 8. The oleosin concentration was set to 0.02 g/L. Data are plotted as mean (n = 3).

at pH 3, which was likely due to increased electrostatic repulsion between oleosins [50], which was in line with the lower interfacial loads found for pH 3 emulsions. The slower adsorption and lower interfacial load, however, did not play a major role in the droplet size distribution after the high-pressure homogenization as shown in Fig. 4.

Based on our experimental observations, we propose a model for the adsorption of oleosins to the emulsion interface during emulsification (Fig. 7a). Before adsorption, the hydrophobic hairpins of oleosins were concealed in the micelles from the aqueous environment due to hydrophobically-driven interactions. When encountering the interface, individual oleosins probably detached from the micelles to adsorb. The dielectric constant of oil (~2) is much lower than that of water (~80), which limited the hydrophobically-driven interactions [52]. Likely, the micelles opened, and the hydrophobic hairpin was inserted into the oil phase. The hydrophilic arms were probably lying on the interface like in native oleosomes, to prevent unfavorable contact between oil and water. The more suitable environment for the hairpins and the reduction of the system's energy by reducing the contact of oil and water together were likely the driving forces for micelle dissociation. A similar interfacial dissociation was previously proposed for hydrophobin multimers [17] and low-density lipoprotein (LDL) from egg yolk [2]. Like oleosins, they form assemblies in water to prevent the exposure of hydrophobic domains, but when they come in contact with a hydrophobic interface, the assemblies disrupt, and individual proteins spread to cover the interface.

The micelles that mainly adsorbed to and dissociated at the interface were likely micelles or small micelle aggregates (<450 nm), similar to what we observed previously under diffusion-controlled conditions [37]. Nanosized aggregates diffused to the interface sufficiently fast to stabilize the droplets during emulsification; while larger aggregates precipitated, which was visually observed after storing the emulsion for 7 days. Therefore, delivering oleosins to the droplet interface was a main hurdle when preparing the emulsions. From the interfacial loads, we calculated that most oleosins remained in aggregates in the continuous phase, and only ~ 2.3 g or 3.5 g oleosins/L emulsion were associated with the interface in E_{pH3} and E_{pH8}, respectively. This was ~ 30% of the determined C_{cr} at both pH's, which explained the low oil:protein ratios that were observed in the previous section for the oleosin emulsions. Most of the added oleosins precipitated and did not adsorb to the interface.

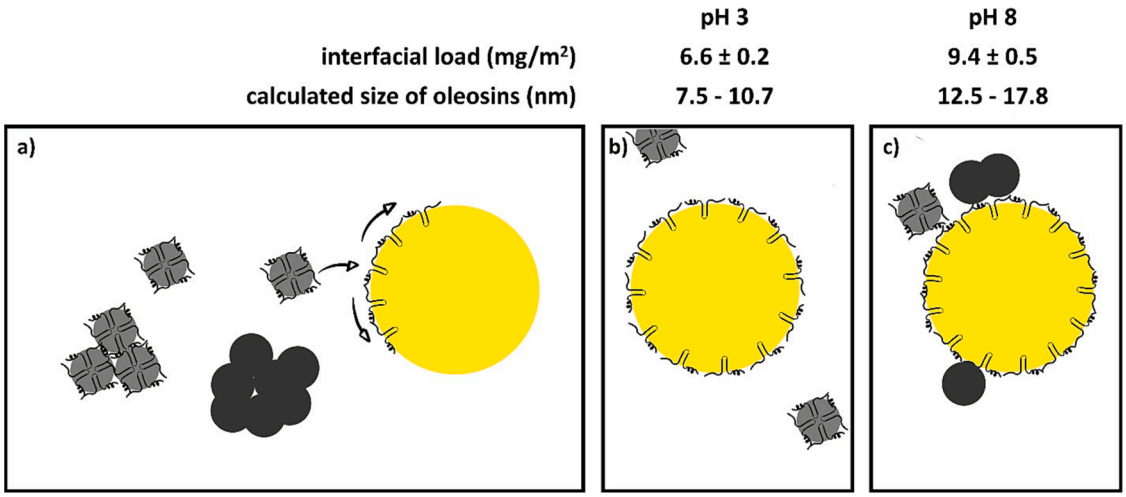

Fig. 7. Schematical models for the adsorption of oleosin aggregates (a) and emulsion droplets at pH 3 (b) and pH 8 (c). In b) and c) the corresponding interfacial loads and calculated sizes of oleosins at the interface are presented. The schematic models are not to scale.

3.4. Stability of oleosin emulsions

Directly after preparation, the droplet size distributions for E_{pH8} and E_{pH3} were monomodal (Fig. 8a), with larger sizes observed for E_{pH8} ($d_{3,2}$ = 5.9 ± 0.7 μm) compared to E_{pH3} ($d_{3,2}$ = 1.6 ± 0.0 μm). The CLSM images of E_{pH8} (Fig. 5c-d) indicated the larger sizes in E_{pH8} were due to droplet flocculation, hence the emulsions were remeasured after mixing with 1 wt% SDS to break flocculates. While at pH 3 no changes occurred after SDS addition, in E_{pH8} the peak shifted to a distribution almost identical to the one of E_{pH3}. This confirmed that the larger sizes in E_{pH8} were flocculates. During 7 days of storage, the size of the flocculates in E_{pH8} as well as of the individual droplets (after SDS addition) at both pH's remained stable (Fig. 8b). To better understand why droplets in E_{pH8} flocculated, the zeta potential of both emulsions was measured. The zeta-potential of E_{pH8} was −15.6 ± 1.2 mV compared to the 28.1 ± 2.1 mV of E_{pH3}. The absolute zeta-potential of E_{pH8} was below 30 mV, which is the common rule of thumb for sufficient charge to prevent flocculation [4].

The stability test confirmed that oleosins protected the droplets from coalescence, while flocculation was only prevented at pH 3 and not at pH 8. The stability of the oleosin stabilized droplets was similar to other protein stabilized emulsions. Proteins commonly form fairly thin interfacial layers (1–10 nm), which protect droplets from coalescing via short-range steric repulsion. And only if the proteins are sufficiently charged, they also prevent flocculation via electrostatic repulsion [28,29,41].

Previously, Tzen and Huang [45] suggested that oleosins are not able to stabilize oil droplets by themselves and that they can prevent droplet coalescence solely in combination with phospholipids. They used an oil: protein ratio of 70 as found in native maize oleosomes, which was likely not enough to ensure that oleosins fully covered the droplet interfaces and hence they had to compensate for the missing oleosins by adding phospholipids. Furthermore, emulsions stabilized only by rapeseed oleosins were reported to easily flocculate [12,51]. The pH values used in those reports were 5.5 or 8, which is in line with our observations; protection against flocculation is only guaranteed at a pH far away from the isoelectric point.

4. Conclusions

In this study, we investigated the emulsification ability and unveiled the emulsification mechanism of isolated oleosins. When dispersed in aqueous buffers, oleosins assemble into micelle-like particles (~33 nm) that further aggregate into particles of up to 20 μm. Micelles aggregate more extensively when oleosins lack charge. Despite, this aggregation isolated oleosins retain their ability to stabilize oil droplets. ~30% of the oleosin aggregates dissociate and individual oleosins adsorb to stabilize the droplet interface. Additionally, micelles and micelle aggregates attach to the droplet interface if the oleosin's charge is insufficient. Oleosins protect droplets from coalescence, while flocculation is only prevented if oleosins are sufficiently charged. The gained insights into the emulsification mechanism of isolated oleosins set the stage for

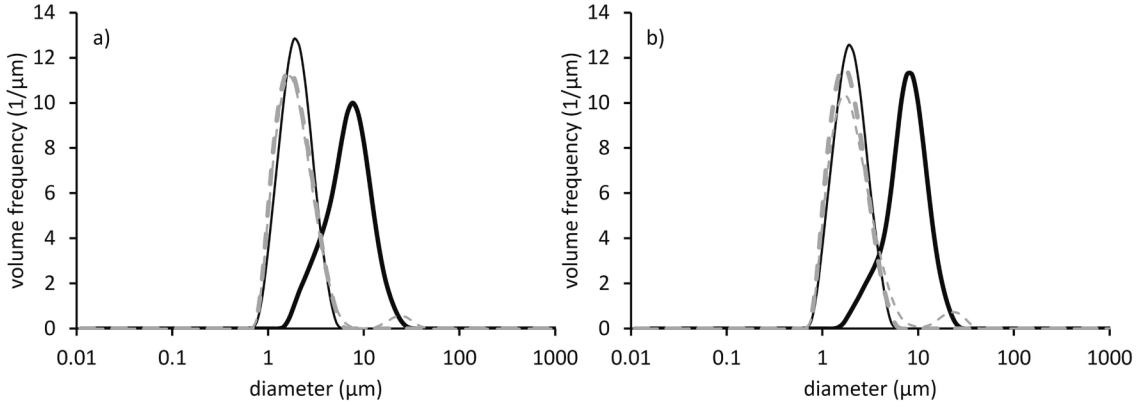

Fig. 8. Size distributions of oleosin emulsions fresh after preparation (a) and after 7 days of storage (b). In grey dashed lines, emulsions are at pH 3, and in black solid lines, emulsions are at pH 8. Thick lines are without and thin lines with SDS addition (1:1 v/v ratio emulsion:SDS solution).

further exploring the unique properties of oleosins.

CRediT authorship contribution statement

Lorenz Plankensteiner: Funding acquisition, Conceptualization, Methodology, Investigation, Formal analysis, Writing – original draft. **Marie Hennebelle:** Funding acquisition, Conceptualization, Supervision, Writing – review & editing. **Jean-Paul Vincken:** Writing – review & editing. **Constantinos V. Nikiforidis:** Funding acquisition, Conceptualization, Methodology, Supervision, Writing – review & editing.

Declaration of Competing Interest

The authors declare the following financial interests/personal relationships which may be considered as potential competing interests: Lorenz Plankensteiner reports financial support was provided by the Dutch Research Council. Lorenz Plankensteiner reports financial support was provided by BOTANECO Inc.

Data availability

Data will be made available on request.

Acknowledgements

The authors thank dr. Laura Schijven and dr. Marlene Führer for collecting the TEM images and Umay Vardar-Kule for collecting the CLSM images. Additionally, we are grateful for the help of dr. Khoa Nguyen's for mathematical questions and dr. Jack Yang for his help with the ADT measurements. This research was funded by the Dutch Research Council (NWO) in the framework of the Green Top Sector Graduate School (GSGT.2019.021) and in collaboration with BOTANECO®.

Appendix A. Supplementary data

Supplementary data to this article can be found online at https://doi.org/10.1016/j.jcis.2023.11.165.

References

[1] J. Aguiar, P. Carpena, J. Molina-Bolıvar, C.C. Ruiz, On the determination of the critical micelle concentration by the pyrene 1: 3 ratio method, J. Colloid Interface Sci. 258 (1) (2003) 116–122.
[2] M. Anton, Egg yolk: structures, functionalities and processes, J. Sci. Food Agric. 93 (12) (2013) 2871–2880.
[3] J. Benjamins, Static and dynamic properties of proteins adsorbed at liquid interfaces, Wageningen University and Research, 2000.
[4] S. Bhattacharjee, DLS and zeta potential–what they are and what they are not? J. Control. Release 235 (2016) 337–351.
[5] M. Blank, B.B. Lee, J.S. Britten, Adsorption kinetics of ovalbumin monolayers, J. Colloid Interface Sci. 50 (2) (1975) 215–222.
[6] A.J. Board, J.M. Crowther, A. Acevedo-Fani, C.-N. Meisrimler, G.B. Jameson, R. C. Dobson, How plants solubilise seed fats: revisiting oleosin structure and function to inform commercial applications, Biophys. Rev. (2022) 1–10.
[7] D. Chandler, Interfaces and the driving force of hydrophobic assembly, Nature 437 (7059) (2005) 640–647.
[8] D.L. Cheung, S. Samantray, Molecular dynamics simulation of protein biosurfactants, Colloids Interfaces 2 (3) (2018) 39.
[9] G. Dalkas, S.R. Euston, Molecular simulation of protein adsorption and conformation at gas-liquid, liquid–liquid and solid–liquid interfaces, Curr. Opin. Colloid Interface Sci. 41 (2019) 1–10.
[10] R.J. Delahaije, H. Gruppen, M.L. Giuseppin, P.A. Wierenga, Quantitative description of the parameters affecting the adsorption behaviour of globular proteins, Colloids Surf. B Biointerfaces 123 (2014) 199–206.
[11] R.J. Delahaije, H. Gruppen, M.L. Giuseppin, P.A. Wierenga, Towards predicting the stability of protein-stabilized emulsions, Adv. Colloid Interface Sci. 219 (2015) 1–9.
[12] M. Deleu, G. Vaca-Medina, J.-F. Fabre, J. Roïz, R. Valentin, Z. Mouloungui, Interfacial properties of oleosins and phospholipids from rapeseed for the stability of oil bodies in aqueous medium, Colloids Surf. B Biointerfaces 80 (2) (2010) 125–132.
[13] S.R. Euston, Molecular simulation of adsorption of hydrophobin HFBI to the air–water, DPPC–water and decane–water interfaces, Food Hydrocoll. 42 (2014) 66–74.
[14] H. Fischer, I. Polikarpov, A.F. Craievich, Average protein density is a molecular-weight-dependent function, Protein Sci. 13 (10) (2004) 2825–2828.
[15] Y. Gohon, J.-D. Vindigni, A. Pallier, F. Wien, H. Celia, A. Giuliani, C. Tribet, T. Chardot, P. Briozzo, High water solubility and fold in amphipols of proteins with large hydrophobic regions: oleosins and caleosin from seed lipid bodies, Biochimica et Biophysica Acta (BBA)-Biomembranes 1808 (3) (2011) 706–716.
[16] A. Guzha, P. Whitehead, T. Ischebeck, K.D. Chapman, Lipid droplets: packing hydrophobic molecules within the aqueous cytoplasm, Annu. Rev. Plant Biol. 74 (2023) 195–223.
[17] J. Hakanpää, G.R. Szilvay, H. Kaljunen, M. Maksimainen, M. Linder, J. Rouvinen, Two crystal structures of Trichoderma reesei hydrophobin HFBI—the structure of a protein amphiphile with and without detergent interaction, Protein Sci. 15 (9) (2006) 2129–2140.
[18] Honaker, L. W., Eijffius, A., Plankensteiner, L., Nikiforidis, C. V., & Deshpande, S. (2023). Biosensing with Oleosin-Stabilized Liquid Crystal Droplets.
[19] C.-Y. Huang, A.H. Huang, Unique motifs and length of hairpin in oleosin target the cytosolic side of endoplasmic reticulum and budding lipid droplet, Plant Physiol. 174 (4) (2017) 2248–2260.
[20] P. Jolivet, L. Aymé, A. Giuliani, F. Wien, T. Chardot, Y. Gohon, Structural proteomics: Topology and relative accessibility of plant lipid droplet associated proteins, J. Proteomics 169 (2017) 87–98.
[21] P. Jolivet, C. Boulard, A. Bellamy, C. Larré, M. Barre, H. Rogniaux, S. d'Andréa, T. Chardot, N. Nesi, Protein composition of oil bodies from mature Brassica napus seeds, Proteomics 9 (12) (2009) 3268–3284.
[22] J.A. Julien, S.G. Mutchek, N.J. Wittenberg, K.J. Glover, Biophysical characterization of full-length oleosin in dodecylphosphocholine micelles, Proteins Struct. Funct. Bioinf. 90 (2) (2022) 560–565.
[23] J.A. Julien, A.L. Pellett, S.S. Shah, N.J. Wittenberg, K.J. Glover, Preparation and characterization of neutrally-buoyant oleosin-rich synthetic lipid droplets, Biochimica et Biophysica Acta (BBA)-Biomembranes 1863 (8) (2021), 183624.
[24] J. Jumper, R. Evans, A. Pritzel, T. Green, M. Figurnov, O. Ronneberger, K. Tunyasuvunakool, R. Bates, A. Žídek, A. Potapenko, Highly accurate protein structure prediction with AlphaFold, Nature 596 (7873) (2021) 583–589.
[25] K. Kalyanasundaram, J. Thomas, Environmental effects on vibronic band intensities in pyrene monomer fluorescence and their application in studies of micellar systems, J. Am. Chem. Soc. 99 (7) (1977) 2039–2044.
[26] O. Leprince, A. Van Aelst, H. Pritchard, D. Murphy, Oleosins prevent oil-body coalescence during seed imbibition as suggested by a low-temperature scanning electron microscope study of desiccation-tolerant and-sensitive oilseeds, Planta 204 (1) (1997) 109–119.
[27] M. Li, L. Smith, D. Clark, R. Wilson, D. Murphy, Secondary structures of a new class of lipid body proteins from oilseeds, J. Biol. Chem. 267 (12) (1992) 8245–8253.
[28] D.J. McClements, Food emulsions: principles, practices, and techniques, CRC Press, 2015.
[29] D.J. McClements, L. Bai, C. Chung, Recent advances in the utilization of natural emulsifiers to form and stabilize emulsions, Annu. Rev. Food Sci. Technol. 8 (2017) 205–236.
[30] D.J. McClements, J. Lu, L. Grossmann, Proposed Methods for Testing and Comparing the Emulsifying Properties of Proteins from Animal, Plant, and Alternative Sources, Colloids Interfaces 6 (2) (2022) 19.
[31] R. Mezzenga, P. Fischer, The self-assembly, aggregation and phase transitions of food protein systems in one, two and three dimensions, Rep. Prog. Phys. 76 (4) (2013), 046601.
[32] D.J. Murphy, The biogenesis and functions of lipid bodies in animals, plants and microorganisms, Prog. Lipid Res. 40 (5) (2001) 325–438.
[33] D.J. Murphy, I. Cummins, Seed oil-bodies: isolation, composition and role of oil-body apolipoproteins, Phytochemistry 28 (8) (1989) 2063–2069.
[34] B.S. Murray, R. Ettelaie, A. Sarkar, A.R. Mackie, E. Dickinson, The perfect hydrocolloid stabilizer: imagination versus reality, Food Hydrocoll. 106696 (2021).
[35] Y. Pan, W. Jin, Q. Huang, Structure, assembly and application of novel peanut oil body protein extracts nanoparticles, Food Chem. 367 (2022), 130678.
[36] C.C. Peng, I.P. Lin, C.K. Lin, J.T. Tzen, Size and stability of reconstituted sesame oil bodies, Biotechnol. Prog. 19 (5) (2003) 1623–1626.
[37] L. Plankensteiner, J. Yang, J.H. Bitter, J.-P. Vincken, M. Hennebelle, C. Nikiforidis, High yield extraction of oleosins, the proteins that plants developed to stabilize oil droplets, Food Hydrocoll. 108419 (2022).
[38] M. Rayner, D. Marku, M. Eriksson, M. Sjöö, P. Dejmek, M. Wahlgren, Biomass-based particles for the formulation of Pickering type emulsions in food and topical applications, Colloids Surf A Physicochem Eng Asp 458 (2014) 48–62.
[39] J. Schindelin, I. Arganda-Carreras, E. Frise, V. Kaynig, M. Longair, T. Pietzsch, S. Preibisch, C. Rueden, S. Saalfeld, B. Schmid, Fiji: an open-source platform for biological-image analysis, Nat. Methods 9 (7) (2012) 676–682.
[40] T.L. Shimada, T. Shimada, H. Takahashi, Y. Fukao, I. Hara-Nishimura, A novel role for oleosins in freezing tolerance of oilseeds in Arabidopsis thaliana, Plant J. 55 (5) (2008) 798–809.
[41] P. Smulders, Formation and stability of emulsions made with proteins and peptides, Wageningen University and Research, 2000.
[42] S. Sridharan, M.B. Meinders, J.H. Bitter, C.V. Nikiforidis, On the emulsifying properties of self-assembled pea protein particles, Langmuir 36 (41) (2020) 12221–12229.
[43] J. Talbot, G. Tarjus, P. Van Tassel, P. Viot, From car parking to protein adsorption: an overview of sequential adsorption processes, Colloids Surf A Physicochem Eng Asp 165 (1–3) (2000) 287–324.

[44] E. Teuling, J.W. Schrama, H. Gruppen, P.A. Wierenga, Characterizing emulsion properties of microalgal and cyanobacterial protein isolates, Algal Res. 39 (2019), 101471.
[45] J. Tzen, A. Huang, Surface structure and properties of plant seed oil bodies, J. Cell Biol. 117 (2) (1992) 327–335.
[46] J. Tzen, G. Lie, A. Huang, Characterization of the charged components and their topology on the surface of plant seed oil bodies, J. Biol. Chem. 267 (22) (1992) 15626–15634.
[47] K.B. Vargo, R. Parthasarathy, D.A. Hammer, Self-assembly of tunable protein suprastructures from recombinant oleosin, Proc. Natl. Acad. Sci. 109 (29) (2012) 11657–11662.
[48] K.B. Vargo, N. Sood, T.D. Moeller, P.A. Heiney, D.A. Hammer, Spherical micelles assembled from variants of recombinant oleosin, Langmuir 30 (38) (2014) 11292–11300.
[49] T. Wahlroos, J. Soukka, A. Denesyuk, P. Susi, Amino-terminus of oleosin protein defines the size of oil bodies-topological model of oleosin-oil body complex, J. Plant Biochem. Physiol. (2015).
[50] P.A. Wierenga, M.B. Meinders, M.R. Egmond, A.G. Voragen, H.H. de Jongh, Quantitative description of the relation between protein net charge and protein adsorption to air– water interfaces, J. Phys. Chem. B 109 (35) (2005) 16946–16952.
[51] C. Wijesundera, T. Boiteau, X. Xu, Z. Shen, P. Watkins, A. Logan, Stabilization of Fish Oil-in-Water Emulsions with Oleosin Extracted from Canola Meal, J. Food Sci., 78(9), C1340-C1347, 2013.
[52] H.-X. Zhou, X. Pang, Electrostatic interactions in protein structure, folding, binding, and condensation, Chem. Rev. 118 (4) (2018) 1691–1741.